CHEMISTRY
A EUROPEAN JOURNAL

FULL PAPER

DOI: 10.1002/chem.201302418

Dysprosium Complexes and Their Micelles as Potential Bimodal Agents for Magnetic Resonance and Optical Imaging

Elke Debroye,[a] Sophie Laurent,[b] Luce Vander Elst,[b] Robert N. Muller,[b, c] and Tatjana N. Parac-Vogt*[a]

Abstract: Six diethylene triamine pentaacetic acid (DTPA) bisamide derivatives functionalized with *p*-toluidine (DTPA-BTolA), 6-aminocoumarin (DTPA-BCoumA), 1-naphthalene methylamine (DTPA-BNaphA), 4-ethynylaniline (DTPA-BEthA), *p*-dodecylaniline (DTPA-BC_{12}PheA) and *p*-tetradecyl-aniline (DTPA-BC_{14}PheA) were coordinated to dysprosium(III) and the magnetic and optical properties of the complexes were examined in detail. The complexes consisting of amphiphilic ligands (DTPA-BC_{12}PheA and DTPA-BC_{14}PheA) were further assembled into mixed micelles. Upon excitation into the ligand levels, the complexes display characteristic Dy^{III} emission with quantum yields of 0.3–0.5% despite the presence of one water molecule in the first coordination sphere. A deeper insight into the energy-transfer processes has been obtained by studying the photophysical properties of the corresponding Gd^{III} complexes. Since the luminescence quenching effect is decreased by the intervention of non-ionic surfactant, quantum yields up to 1% are obtained for the micelles. The transverse relaxivity r_2 per Dy^{III} ion at 500 MHz and 310 K reaches a maximum value of 27.4 $s^{-1}mM^{-1}$ for Dy-DTPA-BEthA and 36.0 $s^{-1}mM^{-1}$ for the Dy-DTPA-BC_{12}PheA assemblies compared with a value of 0.8 $s^{-1}mM^{-1}$ for Dy-DTPA. The efficient T_2 relaxation, especially at high magnetic field strengths, is sustained by the high magnetic moment of the dysprosium ion, the coordination of water molecules with slow water exchange kinetics and long rotational correlation times. These findings open the way to the further development of bimodal optical and magnetic resonance imaging probes starting from single lanthanide compounds.

Keywords: bimodal imaging · dysprosium · micelles · magnetic resonance imaging · luminescence

Introduction

In magnetic resonance imaging (MRI) research, the contrast is predominantly enhanced by agents based on gadolinium coordinated to diethylenetriaminepentaacetic acid (DTPA) or 1,4,7,10-tetraazacyclododecane-1,4,7,10-tetraacetic acid (DOTA) derivatives. Paramagnetic Gd^{III} compounds shorten the longitudinal relaxation time (T_1) of water protons resulting in a positive contrast.[1] The high spatial resolution and tissue penetration of the MRI technique is unfortunately encountered by a low sensitivity. Another drawback is the decrease of the relaxation efficiency with increasing magnetic field strengths. In the past, different strategies have been applied to achieve better magnetic properties. The molecular tumbling rate of contrast agents has been decreased by conjugation of the chelates to macromolecules like linear polymers or dendrimers,[2] by a non-covalent interaction with proteins like human serum albumin[3] or by the incorporation into supramolecular micelles or liposomes.[4] In the latter assemblies, the sensitivity is increased by the accumulation of contrast agents into a small volume. However, an alternative way to improve the MRI efficiency is to shift the focus to the acceleration of the transverse relaxation of water protons (T_2) instead.[5] Particularly in high-field applications, clear images are obtained for negative contrast agents, which are currently mainly based on iron oxide particles.[6]

Recently, probes combining paramagnetic and luminescent features have been created to enhance the imaging performance of contrast agents. The low detection limit of optical imaging provides a high sensitivity together with the good resolution of MR imaging.[7] DTPA and DOTA derivatives have been attached to several organic dyes[8] and transition-metal complexes[9] and their bimodal applications have been exploited. The design and characterization of fluorescent liposomes[10] and nanoparticles enhancing the longitudinal[11] or transverse relaxation time[12] have also been reported. The encountered restrictions of bioconjugates con-

[a] E. Debroye, Prof. T. N. Parac-Vogt
Department of Chemistry, KU Leuven
Celestijnenlaan 200F, 3001 Leuven (Belgium)
Fax: (+32) 16-327992
E-mail: Tatjana.Vogt@chem.kuleuven.be

[b] Prof. S. Laurent, Prof. L. Vander Elst, Prof. R. N. Muller
Department of General Organic and Biomedical Chemistry
University of Mons, Place du Parc 23
7000 Mons (Belgium)

[c] Prof. R. N. Muller
Centre for Microscopy and Molecular Imaging (CMMI)
6041 Gosselies (Belgium)

Supporting information for this article is available on the WWW under http://dx.doi.org/10.1002/chem.201302418.

cerning short luminescence lifetimes, small Stokes shifts, and photobleaching, are all circumvented by the use of lanthanide-based systems. Paramagnetic gadolinium complexes are mixed with UV/Vis or near-infrared (NIR)-emitting lanthanide chelates and since the *f–f* transitions are characterized by low molar absorption coefficients, a conjugated chromophore will serve as an antenna, which transfers the energy of absorbed light to the lanthanide emissive state. This leads to a unique pattern of sharp emission bands while the gadolinium moiety provides high-resolution T_1 weighted images.[13] However, the field of bimodal imaging using one single chelated lanthanide ion is entirely new and attracts much attention.[14]

Here, we present a new concept towards bimodal contrast agents based on a single lanthanide(III) ion by exploiting the unique properties of the dysprosium ion. Dysprosium(III) ions possess a very high magnetic moment ($\mu = 10.2\ \mu_B$) and an asymmetric electronic ground state ($^6H_{15/2}$) and therefore the corresponding compounds display a high transverse relaxivity at high magnetic fields, which makes them suitable for the design of negative (T_2) contrast agents.[15] Moreover, sensitized Dy^{III} ions can emit blue light at about 480 nm, yellow light at about 575 nm[16] and even white light can be obtained by delicate tuning of the blue/yellow intensity ratio. By consequence, both magnetic and optical properties of Dy^{III} chelates make it an interesting candidate for potential bimodal imaging applications.

Recently we reported on a series of four new DTPA bisamide derivatives containing different sensitizing ligands for lanthanide luminescence.[13e] DTPA-bis-*p*-toluidine-amide (DTPA-BTolA), DTPA-bis-6-coumarin-amide (DTPA-BCoumA), DTPA-bis-1-naphthyl-methyl-amide (DTPA-BNaphA) and DTPA-bis-4-ethynylphenyl amide (DTPA-BEthA) chelates were formed with paramagnetic gadolinium and luminescent europium or terbium resulting in complexes with interesting MR/optical imaging properties. In general, Gd-DTPA bisamides are characterized by a slow water exchange or relatively large τ_M values.[17] However, in the case of dysprosium complexes this can have a favorable effect on the magnetic properties as the efficacy of Dy complexes with a relatively long water residence time as negative contrast agents for high-field MRI has previously been demonstrated.[15a]

In this work, a series of Dy^{III} complexes were prepared based on DTPA-BTolA, DTPA-BCoumA, DTPA-BNaphA, DTPA-BEthA, and on two amphiphilic DTPA-bis-*p*-dodecylphenyl-amide or DTPA-bis-*p*-tetradecylphenyl amide ligands. The relaxation and luminescence efficiency of the six dysprosium DTPA bisamide complexes and of the corresponding micelles formed by the amphiphilic ligands have been investigated in detail.

Results and Discussion

Synthesis of ligands, complexes, and micelles: Four DTPA bisamide derivatives with short side chains and two with long hydrophobic side chains are synthesized starting from DTPA bisanhydride. First, DTPA bisanhydride is formed from diethylene triamine pentaacetic acid and acetic anhydride. Consequently, two equivalents of the aromatic amine of interest have been attached through two amide bonds. The obtained ligands DTPA-bis-*p*-toluidine-amide (DTPA-BTolA), DTPA-bis-6-coumarin-amide (DTPA-BCoumA), DTPA-bis-1-naphthylmethyl-amide (DTPA-BNaphA), DTPA-bis-4-ethynylphenyl amide (DTPA-BEthA), DTPA-bis-*p*-dodecylphenyl amide (DTPA-BC_{12}PheA) and DTPA-bis-*p*-tetradecylphenyl amide (DTPA-BC_{14}PheA) are represented in Figure 1. All ligands have been characterized by nuclear magnetic resonance spectroscopy, mass spectrometry, elemental analysis, and IR spectroscopy.[13e]

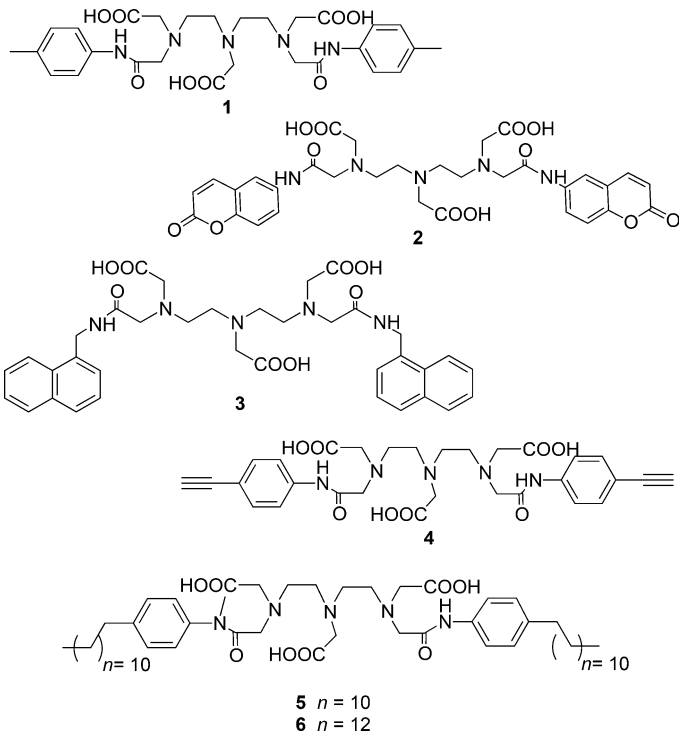

Figure 1. Schematic representation of DTPA-BTolA (**1**), DTPA-BCoumA (**2**), DTPA-BNaphA (**3**), DTPA-BEthA (**4**), DTPA-BC_{12}PheA (**5**), and DTPA-BC_{14}PheA (**6**).

All six ligands are coordinated to dysprosium(III) in water in a mild acidic environment (pH ≈ 6) or in pyridine according to known procedures.[13e,18] The absence of free lanthanide ions is verified by the addition of an arsenazo indicator solution.[19] The complex formation has been established by mass spectrometry, elemental analysis, and IR spectroscopy (Figure S1, the Supporting Information and the Experimental Section). Upon complexation, the C=O acid stretching modes shift 10 to 50 cm^{-1} towards lower wavenumbers, indicating acetate oxygen coordination to the lanthanide ions. Due to the eight-fold coordination of Dy^{III} with the bisamide derivatives (three nitrogen atoms, three acetate oxygen atoms, and two carbonyl oxygen atoms of

the amide groups), thermodynamically stable and kinetically inert complexes are obtained. Referring to previous studies, the ninth coordination site is still available for the reversible binding of a water molecule.[20] Despite the fact that neutral lanthanide DTPA-bisamide chelates are known to be less stable in comparison to their ionic analogues,[21] no release of free dysprosium ions has been observed during the performed experiments.

The dysprosium complexes of DTPA-BC_{12}PheA and DTPA-BC_{14}PheA consist of a hydrophilic center and two hydrophobic tails with a phenyl group and a chain of 12 or 14 carbon atoms. The amphiphilic nature permits them to be incorporated into mixed micelles, creating slowly tumbling supramolecular structures and limiting local motions of the dysprosium complexes. Micelles are formed by mixing 78 mol% phospholipid (DPPC), 15.5 mol% surfactant (Tween 80), and 6.5 mol% of Dy complexes of the ligand of interest. Photon correlation spectroscopy measurements result in homogeneous size distribution profiles. Consequently, the solutions are considered as monodisperse (Figure S2, the Supporting Information). The *Z*-average diameters equal 34.6 and 32.8 nm for the Dy-DTPA-BC_{12}PheA and Dy-DTPA-BC_{14}PheA micelles, respectively. As previously demonstrated, the main factor determining the micelle size is the phospholipid DPPC.[17c]

Photophysical properties: *Dy^{III} complexes*: Due to the $\pi\rightarrow\pi^*$ transitions of the ligands, all dysprosium complexes display well defined absorption bands (Figure 2). For Dy-DTPA-BTolA, the absorption maximum is situated at 245 nm. Dy-DTPA-BCoumA shows an intense absorption band with a maximum at 245 nm, a shoulder at 275 nm, and a low-energy band at 323 nm. The formation of an amide group at the 6-position upon derivatization with DTPA shifts the maximum absorption wavelength of the parent coumarin at 274 nm[22] towards higher energy. The absorption spectrum of Dy-DTPA-BNaphA reveals an intense band at 219 nm and a less-intense band at lower energy between 250–300 nm. The three visible features located at 272, 282, and 291 nm represent the well-known $S_0\rightarrow S_2$ transitions of naphthalene-based ligands.[23] For Dy-DTPA-BEthA, maximum absorption can be seen at 263 nm, corresponding to the phenylethynyl group of the ligand.[24] The absorption spectra of Dy-DTPA-bis-*p*-dodecylphenyl amide and Dy-DTPA-bis-*p*-tetradecylphenyl amide in a 1:1 $CHCl_3$/MeOH mixture are similar and reveal a broad band in the range 240–300 nm with a maximum at approximately 265 nm corresponding to the ligand electronic transitions.

Excitation at the suitable wavelengths (280–330 nm) causes the appearance of characteristic dysprosium emission bands due to $^4F_{9/2}\rightarrow{}^6H_J$ ($J=15/2$–$9/2$) transitions (Figure 3). The band at 483 nm ($^4F_{9/2}\rightarrow{}^6H_{15/2}$) represents a blue color, whereas the more intense $^4F_{9/2}\rightarrow{}^6H_{13/2}$ transition ($\Delta J=2$) at 576 nm reveals a yellow color. The integral intensity of the $^4F_{9/2}\rightarrow{}^6H_{15/2}$ transition decreases from 0.68 to 0.64 relative to the $^4F_{9/2}\rightarrow{}^6H_{13/2}$ transition when going from Dy**1** to Dy**3**. For Dy**4**–**6**, the blue/yellow intensity ratio approaches

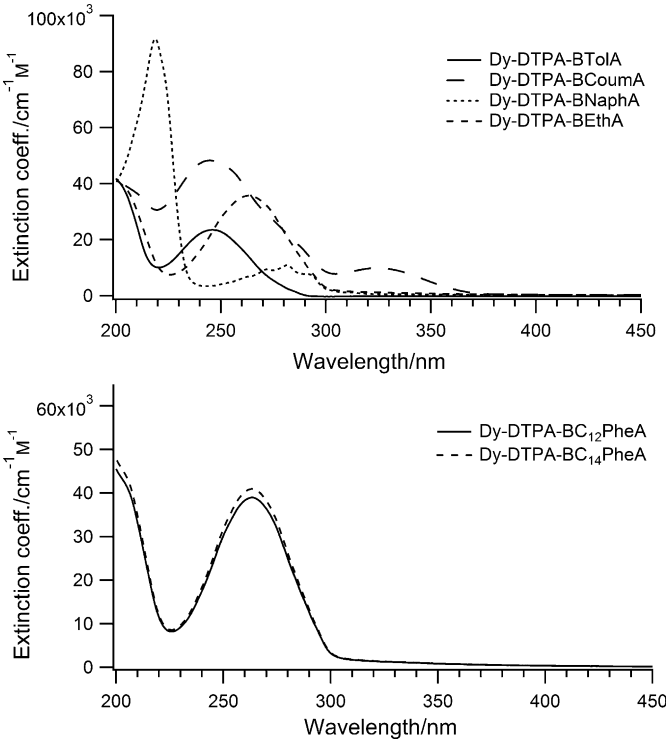

Figure 2. Top: UV/Vis absorption spectra of Dy^{III}-DTPA-BTolA (Dy**1**), Dy^{III}-DTPA-BCoumA (Dy**2**), Dy^{III}-DTPA-BNaphA (Dy**3**) and Dy^{III}-DTPA-BEthA (Dy**4**) in water (pH 7.4, 10^{-4} M, 298 K); Bottom: Dy-DTPA-BC_{12}PheA (Dy**5**) and Dy-DTPA-BC_{14}PheA (Dy**6**) in 1:1 $CHCl_3$/MeOH (10^{-4} M, 298 K).

1 (Table S1, the Supporting Information). The appearance of the $^4F_{9/2}\rightarrow{}^6H_J$ ($J=15/2$–$9/2$) transitions hardly varies with the nature of the ligand. The NIR emission of the dysprosium(III) complexes has also been measured, but no or very low signal has been observed. In general, it is very difficult to observe Dy^{III} NIR luminescence in aqueous solutions due to quenching of the excited states through vibronic coupling with water hydroxyl group vibrations.[25]

Besides, for Dy-DTPA-BNaphA (Dy**3**), ligand-centered emission at lower wavelengths is absent indicating that the ligands are able to efficiently transfer the absorbed energy to the central lanthanide. In the emission spectrum of the Dy**3** complex, the *f*–*f* transitions of the Dy^{III} ion in the range of 470–670 nm are preceded by naphthalene ligand emission (300–510 nm). Such an outcome can be explained by considering the photophysical properties of the Gd**1**–**4** complexes both at room temperature in aqueous solutions and at 77 K in a water/glycerol (9:1) mixture as summarized in Table 1 (Figure S3, the Supporting Information and the Experimental Section). For DTPA-BNaphA, the energy difference between singlet and triplet states is remarkably larger than the ideal value ($\approx$5000 cm^{-1})[26] for efficient intersystem crossing. Concerning the intramolecular energy-transfer, the E_{T1} of DTPA-BTolA and DTPA-BNaphA are 505 and 1220 cm^{-1}, respectively, lower than the resonant $^4F_{9/2}$ level of Dy^{III},[27] so cannot be considered as feeding levels for this ion. Moreover, the ΔE (E_{T1}–$^4F_{9/2}$) for Dy-DPTA-BCoumA

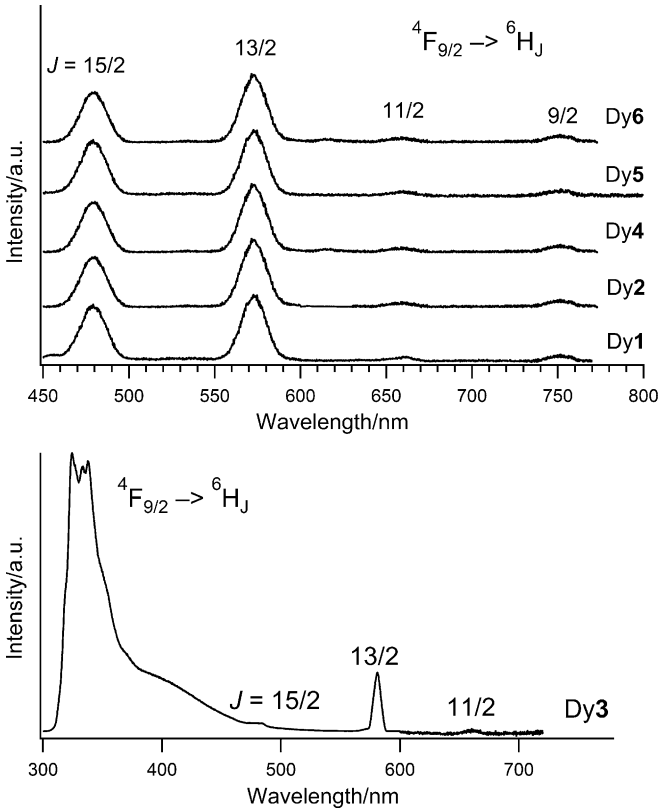

Figure 3. Top: Corrected and normalized emission spectra of Dy^{III}-DTPA-BTolA (Dy**1**), Dy^{III}-DTPA-BCoumA (Dy**2**), and Dy^{III}-DTPA-BEthA (Dy**4**) in water, and Dy-DTPA-BC_{12}PheA (Dy**5**) and Dy-DTPA-BC_{14}PheA (Dy**6**) in 1:1 $CHCl_3$/MeOH; Bottom: Dy^{III}-DTPA-BNaphA (Dy**3**) in water (10^{-4} M, 298 K).

Table 1. Ligand-centered photophysical properties.[13e]

	E_{S1} [cm^{-1}][a]	E_{T_1} [cm^{-1}][b]	ΔE [cm^{-1}]	$(E_{T_1}-{}^4F_{9/2})$ [cm^{-1}]
Gd**1**	26670	20325	6375	−505
Gd**2**	26385	21460	4925	620
Gd**3**	31450	19610	11845	−1220
Gd**4**	27000	22000	5000	1170

[a] Singlet state energy, determined from the edge of the absorption spectra. [b] Triplet state energy, determined as the 0–0 transition from the phosphorescence spectra of the Gd^{III} complexes.

and Dy-DTPA-BEthA is not large enough to exclude back energy transfer from $^4F_{9/2}$ to the ligand triplet state at room temperature.

Luminescence decay curves of all Dy**1**–**4** complexes in H_2O and D_2O have been fitted by a single exponential mode, confirming that the chemical environment of the dysprosium ions is uniform within the complex solutions. As depicted in Table 2, luminescence lifetimes in H_2O increase from 7.6 up to 11.3 μs at the emission wavelength of 576 nm in the row Dy**1** < Dy**3** < Dy**2** < Dy**4**. In D_2O, luminescence lifetimes of 20.2 to 58.3 μs are achieved. Within the uncertainty of the luminescence method, the following phenomenological Equation (1) for Dy^{III}-polyaminocarboxylate systems[28] has been employed to determine the number of coordinated water molecules q with an accuracy of ±0.2–0.3:

Table 2. Photophysical data for the Dy^{III} complexes in water (pH 7.4, 10^{-4} M) and in 1:1 $CHCl_3$/MeOH (10^{-4} M) at 298 K.

	λ_{exc} [nm]	τ_{H_2O} [μs]	τ_{D_2O} [μs]	q_{H_2O}	Q^L_{Dy} [%][c]
Dy**1**[a]	280	7.6 (±0.1)	20.2 (±0.1)	1.1	0.27[d]
Dy**2**[a]	330	9.9 (±0.2)	32.4 (±0.3)	0.9	0.38[d]
Dy**3**[a]	292	9.1 (±0.3)	28.9 (±0.2)	1.0	0.32[e]
Dy**4**[a]	290	11.3 (±0.2)	58.3 (±0.4)	0.9	0.46[e]
Dy**5**[b]	290	20.2 (±0.5)			
Dy**6**[b]	290	20.8 (±0.5)			

[a] In water; [b] in 1:1 $CHCl_3$/MeOH; [c] estimated relative errors: Q^L_{Dy}, ±10%; [d] quantum yield relative to quinine sulphate in 1N H_2SO_4; [e] quantum yield relative to rhodamine 101 in EtOH.

$$q_{Dy}(H_2O) = 21.1\Delta k_{obs} - 0.60 \quad (1)$$

in which $\Delta k_{obs} = 1/\tau_{H_2O} - 1/\tau_{D_2O}$ is expressed in μs^{-1}. After calculation, q_{Dy} (H_2O) values of 0.9–1.1 are obtained. This is in agreement with measurements performed on the corresponding Eu^{III} complexes revealing hydration numbers in the range of 1.0–1.2 water molecules.[13e] Unless the presence of a water molecule in the first coordination sphere, the τ_{H_2O} values are higher in comparison with other Dy^{III} complexes reported in published works.[29] Moreover, lifetimes of 20.2 and 20.8 (±0.5) μs in 1:1 $CHCl_3$/MeOH are obtained for Dy**5** and Dy**6**, respectively. Dy^{III} luminescence quantum yields determined under ligand excitation have been calculated to be between 0.27 and 0.46% for Dy**1**–**4**, which are higher values than other dysprosium complexes with a comparable ligand coordination environment.[29a,c] Referring to Table 1, not only the generally accepted triplet-to-lanthanide energy-transfer, but also sensitization of Dy^{III} emission through the singlet states of DTPA-BTolA and DTPA-BNaphA should be considered. In case of Dy-BTolA, a small shoulder from 448 to 460 nm due to Dy^{III} transitions originating from a group of levels situated around 25800–26000 cm^{-1} such as $^4F_{7/2}$ and $^4I_{13/2}$ and terminating at the $^6H_{13/2}$ level could be observed in the emission spectrum, giving an indication of the involvement of the ligand singlet state (26670 cm^{-1}) in the energy-transfer process.

Micelles: The Dy-DTPA-BC_{12}PheA and Dy-DTPA-BC_{14}PheA complexes are assembled with the phospholipid DPPC and surfactant Tween 80 forming micelles. As shown in Figure 4, a very similar ligand-centered band in the range 240–300 nm with a maximum at 264 nm is observed in the absorption spectrum of the supramolecular structures.

The emission spectra of the micelles display sharp emission bands attributed to the $^4F_{9/2} \rightarrow {}^6H_J$ (J = 15/2–9/2) transitions of the Dy^{III} ion upon excitation at 290 nm (Figure 5). The efficient energy transfer from ligand to lanthanide is maintained since no ligand-centered emission is detected. The relative integral intensities of the $^4F_{9/2} \rightarrow {}^6H_{15/2}$ transition

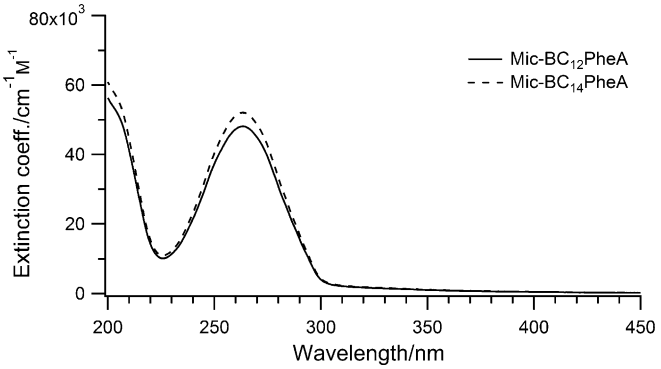

Figure 4. UV/Vis absorption spectra of micelles consisting of Dy-DTPA-BC_{12}PheA and Dy-DTPA-BC_{14}PheA in water (pH 7.4, 10^{-4} M, 298 K).

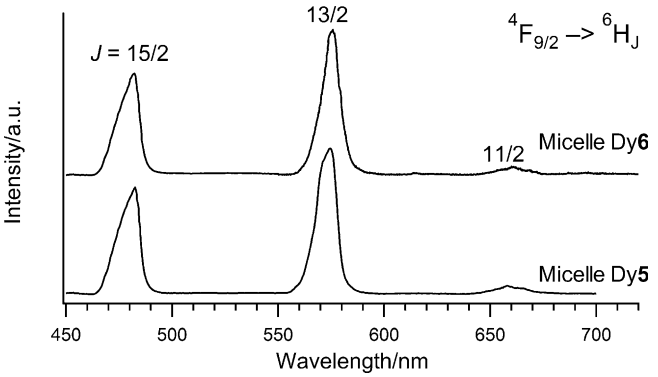

Figure 5. Corrected and normalized emission spectra of micelles consisting of Dy-DTPA-BC_{12}PheA (Micelle Dy**5**) and Dy-DTPA-BC_{14}PheA (Micelle Dy**6**) in water (pH 7.4, 10^{-4} M, 298 K).

with respect to the $^4F_{9/2} \rightarrow {}^6H_{13/2}$ transition follow the same trend as observed for the corresponding complexes that are not incorporated into micelles. For both assemblies, the relative intensity for the blue emission at 483 nm is within 20% smaller than the one for the yellow emission at 576 nm, confirming similarity of the local microenvironment around the dysprosium ions (Table S2, the Supporting Information). The marginal changes upon assembly indicate a low influence of the nature of the environment onto the Dy^{III} emission profile.

Luminescence lifetimes in both H_2O and D_2O have been obtained after a mono-exponential fit of the luminescence decays, which indicates the presence of only one luminescent lanthanide species in the micellar structures. Luminescence lifetimes in H_2O equal 26.7 and 28.2 μs for micelles consisting of Dy-DTPA-BC_{12}PheA and Dy-DTPA-BC_{14}PheA, respectively. In D_2O, luminescence lifetimes up to 0.12 and 0.19 ms are obtained. The number of coordinated water molecules using Equation (1) is calculated to be 0.1 (Table 3). For the sake of comparison, q_{Eu} values of 0.1 are obtained after luminescence lifetime measurements on corresponding micelles containing Eu-DTPA-BC_{12}PheA, and Eu-DTPA-BC_{14}PheA.[30] The remarkably high lifetime values and rather low hydration numbers can be explained

Table 3. Photophysical data for the micelles containing Dy**5** and Dy**6** complexes in water (pH 7.4, 10^{-4} M, 298 K).

	λ_{exc} [nm]	τ_{H_2O} [μs]	τ_{D_2O} [μs]	q_{H_2O}	Q^L_{Dy} [%][a]
Dy**5**	290	26.7 (±0.1)	115.1 (±0.2)	0.0	0.92
Dy**6**	290	28.2 (±0.2)	188.6 (±0.1)	0.1	1.05

[a] Quantum yield relative to quinine sulfate in 1N H_2SO_4; estimated relative errors: Q^L_{Dy}, ±10%.

by the composition of the micelles. The non-ionic surfactant Tween 80 at the periphery of the assembled structures is able to form hydrogen bonds with H_2O and acts as a competitor in lanthanide coordination. Less non-radiative deactivation due to O–H vibrations will take part, leading to longer luminescence lifetimes and as a consequence to a reduced q number found by the phenomenological Equation (1).[31] Dysprosium(III) luminescence quantum yields are determined by excitation at 290 nm into the ligand levels. Values of 0.92 and 1.05% are obtained for the micelles consisting of Dy**5** and Dy**6**, respectively. Compared with other reported dysprosium complexes,[29a,c] exceptionally high absolute quantum yields are established because of the insertion of the luminescent chelates into supramolecular assemblies.[31b]

Relaxometric studies: *Proton longitudinal relaxation rate*: The enhancement of the relaxation rate by 1 mM of the Dy^{III} compound determines the proton longitudinal relaxivity (r_1). In Figure 6, the proton longitudinal relaxivities of Dy**1**–**4**

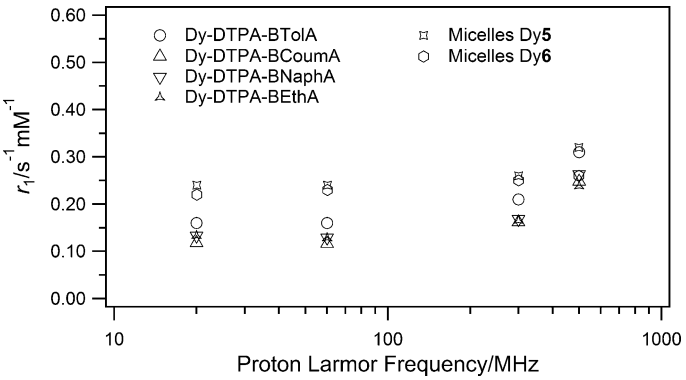

Figure 6. Proton longitudinal relaxivity of the Dy-DTPA bisamides and micelles versus proton Larmor frequency at 310 K.

and the micelles consisting of Dy**5** and Dy**6** at 20, 60, 300, and 500 MHz are depicted. It can be seen that the profiles of the six compounds all follow the same trend. At low magnetic fields (20-60 MHz), low r_1 values of 0.12–0.16 $mM^{-1}s^{-1}$ for Dy**1**–**4** and 0.22–0.24 $mM^{-1}s^{-1}$ for Dy**5**–**6** assemblies are obtained. At higher magnetic fields (300–500 MHz), a slight increase of r_1 to 0.3 $mM^{-1}s^{-1}$ is observed.

Both inner- ($1/T_1^{is}$) and outer-sphere ($1/T_1^{os}$) contributions to the proton longitudinal relaxation rate are defined by the sum of dipolar ($1/T_1^{DD}$) and Curie ($1/T_1^{C}$) contributions. At

low magnetic fields, the longitudinal relaxation rate is mainly modulated by the dipolar interactions between the water proton nuclei and the static magnetic moment arising from the electrons of Dy^{III}, being highly dependent on the electronic relaxation time τ_S.[15a,d] Those findings explain the low r_1 values in this region since Dy^{III} is characterized by a very short τ_S (~0.5 ps).[15a,32] At high magnetic fields, the Curie inner- and outer-sphere contributions become more significant. These terms are modulated by the rotational correlation time of the compound τ_R and the translational correlation time τ_D; τ_D equals a^2/D, in which a is the distance of closest approach between the water protons and the paramagnetic center, and D is the relative diffusion constant of the water molecules moving from the coordination sphere to the bulk water. The proton longitudinal relaxivity will thus slightly increase at higher fields. In the whole range, the longer rotational correlation time of the supramolecular micelles leads to a slightly enhanced longitudinal relaxation rate. It has been found that the outer-sphere contribution predominates the T_1 efficiency of Dy-based paramagnetic compounds.

Proton transverse relaxation rate: Figure 7 depicts the T_2 enhancement at 20, 60, 300, and 500 MHz by the Dy**1**–**4** complexes and the micelles consisting of Dy**5** and Dy**6** in comparison with the data of Dy-DTPA and Dy-DTPA-bis-*n*-butylamide (Dy-DTPA-BnBA).[15a] At the proton Larmor frequency of 20 MHz, the transverse relaxivities for the Dy**1**–**3** complexes are similar to the longitudinal values ($r_2 \approx 0.2$–$0.6\ mM^{-1}s^{-1}$). Dy-DPTA-BEthA and the micellar assemblies of Dy**5** and Dy**6** already reach transverse relaxation rates of 1.8, 1.9, and 1.1 $mM^{-1}s^{-1}$, respectively, at 20 MHz. This is due to the aggregation of the complexes into supramolecular structures. At higher fields ($\nu_o > 100$ MHz), a remarkable increase of r_2 takes place. Besides the fact that the transverse relaxivity depends on the square of the magnetic field, r_2 shows a strong reliance to the τ_M value when the external magnetic field is increased. In that particular case, it is important that the chemical shift difference between coordinated and bulk water ($\Delta\omega_M$) remains slow compared with the water exchange.[15a] The chemical shift of the coordinated water molecule is proportional to the magnetic field and is the sum of contact and pseudo-contact terms.

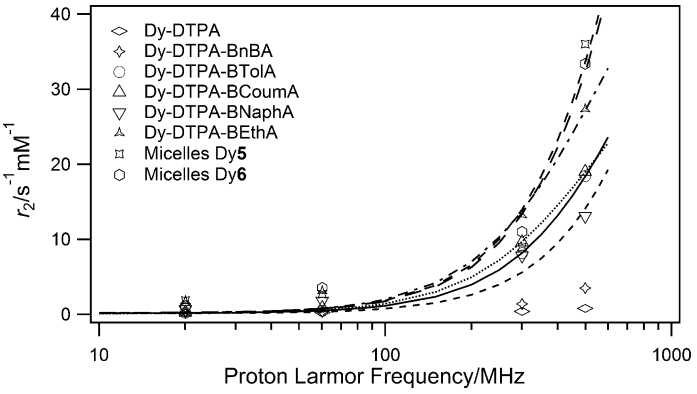

Figure 7. Proton transverse relaxivity of the Dy-DTPA bisamides and micelles versus proton Larmor frequency compared with Dy-DTPA and Dy-DTPA-BnBA at 310 K. The dashed lines represent the fitted data.

Fitting of the data is performed using the Equations defining the inner- and outer-sphere contributions as described by Vander Elst et al.[15a] The inner-sphere contribution depends on the ratio of [Dy complex]/[water], the value of q, the water exchange rate τ_M and the transverse relaxation rate of the coordinated water molecule, $1/T_{2M}$. The latter factor results from dipolar, dipolar Curie, and Curie contact contributions. The correlation time τ_C modulating the dipolar interaction, is related to τ_R, τ_S, and τ_M through $\tau_C^{-1} = \tau_R^{-1} + \tau_S^{-1} + \tau_M^{-1}$. During the fitting procedure, the following parameters were fixed: $q = 1$, $r = 0.31$ nm, $a = 0.36$ nm, $D = 3.3 \times 10^{-9}\ m^2 s^{-1}$. The parameters τ_S, τ_R, τ_M, and $\Delta\omega_M$ are extracted from the fitting and are listed in Table 4. The τ_S values lie in the range of 0.2–0.3 ps, which is in full agreement with $Dy(DTPA)^{2-}$ (0.15 ps). Nuclear magnetic relaxation dispersion (NMRD) measurements on the corresponding Gd**1**–**4** complexes indicated a rotational correlation time τ_R going from 90 ps for Gd**1** to 400 ps for Gd**4**.[13e] The same trend is observed for the described dysprosium complexes. The τ_R values for Dy**1** and Dy**2** equal 97.2 and 115.0 ps, respectively, and are very similar to those obtained for Gd**1** (90 ps) and Gd**2** (115 ps). Analogous to the Gd compounds, Dy-DTPA-BNaphA and Dy-DTPA-BEthA display very high τ_R-values because of intermolecular stacking of the aromatic substituents. The τ_M values of the Dy complexes lie in the range of 150–430 ns and are in general 5 to 6 times shorter than those of the corresponding Gd complexes. Moreover, the water exchange is rather fast compared with the chemical shift difference ($\tau_M^2 \Delta\omega_M^2 < 0.1$). The rates increase in the order Dy**3** < Dy**1**, Dy**4** < Dy**2**, which is expressed in a large enhancement of the transverse relaxation rate as can be seen in Figure 7 (12.9–27.4 $mM^{-1}s^{-1}$ at 500 MHz, 310 K). A clear improvement of relaxation efficiency is obtained compared with previously studied Dy-DPTA and Dy-DTPA-BnBA, which reached maximum transverse relaxivities of less than 4 $mM^{-1}s^{-1}$, at 500 MHz and 310 K.

Table 4. Values of τ_S, τ_R, τ_M, and $\Delta\omega_M$ obtained by fitting of the ^1H r_2 data of the Dy complexes at 310 K.

	τ_S [ps]	τ_R [ps]	τ_M [ns]	$\Delta\omega_M$ [10^5 rad s^{-1} T^{-1}]
Dy**1**	0.240	97.2	275.0	1.92
Dy**2**	0.170	115.0	427.0	1.79
Dy**3**	0.194	300.0	150.0	2.04
Dy**4**	0.194	500.0	291.0	2.58
Dy**5**	0.300	1000.0	100.0	4.04[a]/5.43[b]
Dy**6**	0.300	1000.0	100.0	3.93[a]/7.45[c]

[a] Fitting value with q set to 1; [b] q set to 0.4; [c] q set to 0.6.

Fitting the proton NMRD profiles of micelles consisting of the corresponding Gd**5** and Gd**6** complexes indicated the presence of 0.4 to 0.6 water molecules in the first coordination shell of the lanthanide ion. Despite a reduction of the luminescence quenching effect induced by interactions of Tween 80, a certain amount of coordinated water molecules can still be monitored in MR measurements. During the fitting of the transverse relaxation rates of the Dy-micelles, q was set to 1, as well as to 0.4 for Dy**5** and 0.6 for Dy**6**. Due to the relatively high r_2 values at low fields (20–60 MHz), extra parameters had been fixed to obtain a good match between the fitted and the experimental data. The best results were achieved by adjusting τ_S to 0.3 ps, τ_R to 1 ns and τ_M to 100 ns. The slow molecular motion leads to transverse relaxivities of 36.0 $mM^{-1}s^{-1}$ for the micelles containing Dy**5** complexes and 33.4 $mM^{-1}s^{-1}$ for those built up with Dy**6**. The Curie spin relaxation is prevailingly expressed as an inner-sphere effect. Consequently, the performance as a good r_2 agent is enforced by the high magnetic moment of the dysprosium ion ($\mu = 10.2\ \mu_B$), the presence of a water molecule in the first coordination sphere, slow water exchange kinetics and especially in the case of the micelle assemblies, a long rotational correlation time.[15d]

Given that tissues display a shorter T_2 than T_1, T_2 agents with significant r_2/r_1 ratios can be beneficial by using appropriate pulse sequences in clinical applications. In Figure 8,

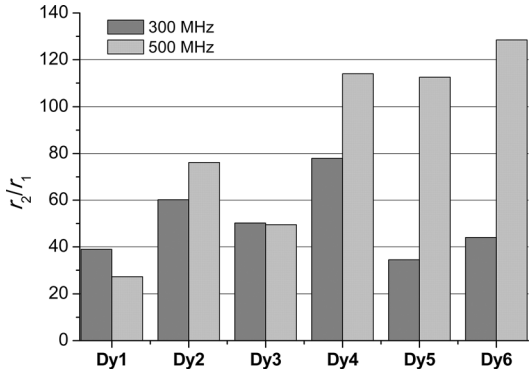

Figure 8. Ratio of proton transverse versus longitudinal relaxivity at 300 and 500 MHz for all six Dy compounds at 310 K.

the r_2/r_1 ratios at 300 and 500 MHz for all discussed compounds are depicted. Except for Dy-DTPA-BTolA and Dy-DTPA-BNaphA, the r_2/r_1 ratio increases going from 300 to 500 MHz. With low r_1 values, the Dy-DTPA-BEthA complex has very large r_2/r_1 ratios, making the compound very efficient at 300 MHz in comparison to the micelles, which gain importance at higher fields.

Each micelle of about 34 nm consisting of a mixture of DPPC phospholipids and Dy^{III} complexes, comprises at least 50 compounds.[17a] The assembly starts from 1 Dy^{III} complex per 12 DPPC molecules, resulting in a minimum load of four dysprosium complexes per micelle. The calculated transverse relaxivity per particle at 300 and 500 MHz is represented in Figure 9. At 500 MHz, the efficiency of the Dy-

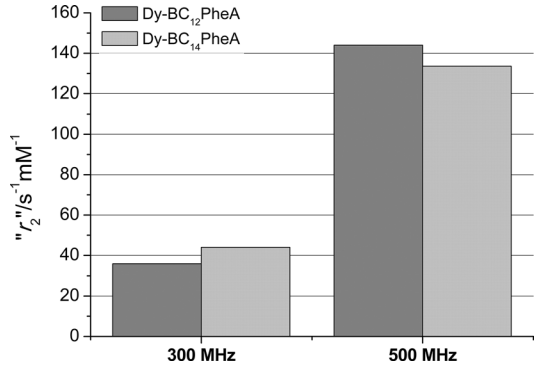

Figure 9. Transverse relaxivity per micelle based on Dy-DTPA-BC_{12}PheA and Dy-DTPA-BC_{14}PheA at 300 and 500 MHz.

DTPA-BC_{12}PheA assemblies is the highest reported in this study, with a per micelle T_2 relaxivity of 144.0 $mM^{-1}s^{-1}$, compared with 133.6 $mM^{-1}s^{-1}$ for the micelles consisting of Dy-DTPA-BC_{14}PheA.

Conclusion

Dysprosium(III) complexes and micelles reported in this study are endowed with favourable magnetic and optical properties making them interesting candidates for potential MR and optical imaging. Despite the accessibility of water to the first coordination sphere, the Dy**1**–**4** complexes and the micelles consisting of Dy**5** and Dy**6** revealed long luminescence lifetimes in H_2O at the emission wavelength of 576 nm and larger Dy^{III} luminescence quantum yields are obtained in comparison to previously reported dysprosium derivatives. Taking into account the photophysical data extracted from measurements on the corresponding Gd^{III}-complexes, not only the ligand triplet states, but also the singlet states are involved into the energy-transfer process. The complexes and especially the micelles exhibit very high transverse relaxivities r_2 of up to 36.0 $s^{-1}mM^{-1}$ at 500 MHz and 310 K, which is clearly superior relative to a r_2 value of 0.8 $s^{-1}mM^{-1}$ for Dy-DTPA. The high transverse relaxivity is mainly due to the increase of the rotational correlation time and the fast water exchange, especially at high magnetic fields. In general, the Dy^{III} micellar assemblies form supramolecular structures with both high relaxivity values and unique luminescent properties.

Experimental Section

Materials: Reagents and solvents were obtained from Sigma–Aldrich (Bornem, Belgium), Acros Organics (Geel, Belgium), ChemLab (Zedelgem, Belgium), Matrix Scientific (Columbia, USA) and BDH Prolabo (Leuven, Belgium), and were used without further purification. Dysprosium(III) chloride hexahydrate was obtained from Sigma–Aldrich (Bornem, Belgium).

Instrumentation: Elemental analysis was performed by using a CE Instruments EA-1110 elemental analyzer. ^1H and ^{13}C NMR spectra were re-

corded by using a Bruker Avance 300 spectrometer (Bruker, Karlsruhe, Germany), operating at 300 MHz for ^{1}H and 75 MHz for ^{13}C, or on a Bruker Avance 400 spectrometer, operating at 400 MHz for ^{1}H and 100 MHz for ^{13}C. IR spectra were measured by using a Bruker Vertex 70 FT-IR spectrometer (Bruker, Ettlingen, Germany). Mass spectra were obtained by using a Thermo Finnigan LCQ Advantage mass spectrometer. Samples for the mass spectrometry were prepared by dissolving the product (2 mg) in methanol (1 mL), then adding 200 μL of this solution to a water/methanol mixture (50:50, 800 μL). The resulting solution was injected at a flow rate of 5 $\mu L\,min^{-1}$. The metal contents were detected on a Varian 720-ES ICP optical emission spectrometer with reference to a Chem-Lab dysprosium standard solution (1000 $\mu g\,mL^{-1}$, 2–5% HNO_3). Solutions were dispersed in a 180 W Bandelin Sonorex RK 510 H sonicator equipped with a thermostatic heating bath. Absorption spectra were measured on a Varian Cary 5000 spectrophotometer on freshly prepared aqua solutions in quartz Suprasil cells (115F-QS) with an optical pathlength of 0.2 cm. The emission spectra of the Gd^{III} complexes at room and liquid nitrogen temperature were measured on a Horiba Jobin Yvon Fluorolog 3 spectrofluorimeter. At 298 K, UV excitation into lower energy bands results in ligand-centered broad-band emission arising mainly from $^{1}\pi\pi^{*}$ states. At 77 K upon enforcing a time delay of 100 μs, the emission from the singlet state disappears giving rise to the triplet state $^{3}\pi\pi^{*}$ emission at lower energy. Emission spectra and luminescence decays of Dy^{III} complexes were recorded on an Edinburgh Instruments FS920 steady state spectrofluorimeter. This instrument is equipped with a 450 W xenon arc lamp, a high energy microsecond flashlamp μF900H and an extended red-sensitive photomultiplier (185–1010 nm, Hamamatsu R 2658P). All spectra are corrected for the instrumental functions. Luminescence decays were determined under ligand excitation (280–330 nm) monitoring emission of the $^{4}F_{9/2}\rightarrow{}^{6}H_{13/2}$ transition for Dy^{III} complexes. Luminescence decays were analyzed using Edinburgh software; lifetimes are averages of at least three measurements. Quantum yields were determined by a comparative method with a standard reference;[33] estimated experimental errors for quantum yield determination ±10%. Quinine sulfate (Fluka) in 1N sulfuric acid ($Q=54.6\%$) was used as a standard for the DTPA-BTolA, DTPA-BCoumA and DTPA-BEthA complexes and for the micelles consisting of Dy-DTPA-BC_{12}PheA and Dy-DTPA-BC_{14}PheA. Rhodamine 101 (Sigma) in ethanol ($Q=100\%$) was used as a standard for the DTPA-BNaphA and DTPA-BEthA complexes.[33] Solutions with a concentration of about 10^{-5} M were prepared to obtain an optical density lower than 0.05 at the excitation wavelength.

Relaxometry: ^{1}H T_1 and T_2 measurements were performed at 37 °C at 0.47, 1.41, 7.05, and 11.75 T on Minispec mq-20, mq-60, Avance-300 and Avance-500 from Bruker, respectively.

DLS measurements: Photon correlation spectroscopy was performed at room temperature with a BIC multiangle laser light-scattering system with a 90° scattering angle (Brookhaven Instruments Corporation, Holtsville, USA). The intensity weighted micellar diameter was measured on 1.10^{-4} M diluted suspensions and calculated by a non-negatively constrained least-squares (multiple pass) routine.

Synthesis: DTPA-bisanhydride, ligands **1**–**4** and the corresponding complexes Dy**1**–**4** were synthesized as described previously.[13e]

Dy^{III}-DTPA-BTolA (Dy1): Yield: 66%. IR: $\tilde{\nu}_{max}=1598$ (COO^{-} asym. stretch), 1506 (amide II), 1394 cm^{-1} (COO^{-} sym. stretch); UV/Vis (water): λ_{max} (ε): 246 nm ($23\,500\ cm^{-1}M^{-1}$); ESI-MS: m/z calcd for $C_{28}H_{34}DyN_5O_8$: 754.1 $[M+Na]^{+}$, found 754.8 $[M+Na]^{+}$; elemental analysis calcd (%) for $C_{28}H_{34}DyN_5O_8$: C 46.00, H 4.69, N 9.58; found: C 45.83, H 4.76, N, 9.51.

Dy^{III}-DTPA-BCoumA (Dy2): Yield: 59%. IR: $\tilde{\nu}_{max}=1563$ (COO^{-} asym. stretch), 1487 (amide II), 1435 cm^{-1} (COO^{-} sym. stretch); UV/Vis (water): λ_{max} (ε): 245 (48 300), 324 nm ($9900\ cm^{-1}M^{-1}$); ESI-MS: m/z calcd for $C_{32}H_{30}DyN_5O_{12}$: 862.1 $[M+Na]^{+}$, found 862.5 $[M+Na]^{+}$; elemental analysis calcd (%) for $C_{32}H_{30}DyN_5O_{12}$: C 45.80, H 3.60, N 8.35; found: C 45.73, H 3.67, N 8.32.

Dy^{III}-DTPA-BNaphA (Dy3): Yield: 67%. IR: $\tilde{\nu}_{max}=1592$ (COO^{-} asym. stretch), 1512 (amide II), 1400 cm^{-1} (COO^{-} sym. stretch); UV/Vis (water): λ_{max} (ε): 219 (91 600), 272 (9400), 282 (10 850), 291 nm ($7700\ cm^{-1}M^{-1}$); ESI-MS: m/z calcd for $C_{36}H_{38}DyN_5O_8$: 854.2 $[M+Na]^{+}$, 1685.4 $[2M+Na]^{+}$, found 855.2 $[M+Na]^{+}$, 1687.0 $[2M+Na]^{+}$; elemental analysis calcd (%) for $C_{36}H_{38}DyN_5O_8$: C 52.02, H 4.61, N 8.43; found: C 51.72, H 4.69, N 8.24.

Dy^{III}-DTPA-BEthA (Dy4): Yield: 58%. IR: $\tilde{\nu}_{max}=1584$ (COO^{-} asym. stretch), 1509 (amide II), 1396 cm^{-1} (COO^{-} sym. stretch); UV/Vis (water): λ_{max} (ε): 263 nm ($35\,750\ cm^{-1}M^{-1}$); ESI-MS: m/z calcd for $C_{30}H_{30}DyN_5O_8$: 774.1 $[M+Na]^{+}$, found 773.9 $[M+Na]^{+}$; elemental analysis calcd (%) for $C_{30}H_{30}DyN_5O_8$: C 47.79, H 4.03, N 9.32; found: C 47.53, H 4.10, N 9.25.

Ligands DTPA-BC_{12}PheA (5) and DTPA-BC_{14}PheA (6) according to a slightly modified procedure:[17c,34] *p*-Dodecylaniline (0.52 g, 2 mmol, 2 equiv) or *p*-tetradecylaniline (0.58 g, 2 mmol, 2 equiv) were dissolved in $CHCl_3$ (30 mL). The solution was brought to 40 °C and then added dropwise to a solution of DTPA-bisanhydride (0.36 g, 1 mmol, 1 equiv) in dry DMF (40 mL, 40 °C). The reaction mixture was stirred for eight hours at 50 °C after which the solvents were removed. To the yellowish powder, acetone (20 mL) was added and the suspension was filtered over a Büchner. The pale compound was washed with acetone (2×20 mL) and was dried overnight in vacuo at 50 °C. The powder was stirred in water (150 mL) at 80 °C during three hours to dissolve excess of DTPA. After filtration, the residue was washed with acetone (2×20 mL) again and brought to reflux conditions in $CHCl_3$ (150 mL) for another three hours. A creamy white powder was finally obtained after filtration and rinsing with acetone (2×20 mL). The pure compound was dried overnight in vacuo at 50 °C.

DTPA-BC_{12}PheA: Yield: 0.55 g, 62%; ^{1}H NMR (400 MHz, CD_3OD, 25 °C, TMS): $\delta=0.92$ (t, 6H, CH_3), 1.29 (m, 44H, alkyl CH_2), 2.06, 2.19 (t, 8H, N-CH_2-CH_2-N), 2.91, 2.98, 3.51 (s, 10H, N-CH_2-C(O)), 7.02 (d, 2H, phenyl C*H*), 7.38 (d, 4H, phenyl C*H*), 7.54 ppm (d, 2H, phenyl C*H*); IR: $\tilde{\nu}_{max}=1626$ (C=O free acid), 1529 cm^{-1} (C=O amide); ESI-MS: m/z calcd for $C_{50}H_{81}N_5O_8$: 926.2 $[M+2Na]^{+}$, 949.2 $[M+3Na]^{+}$; found: 925.6 $[M+2Na]^{+}$, 947.0 $[M+3Na]^{+}$; elemental analysis calcd (%) for $C_{50}H_{81}N_5O_8{\cdot}H_2O$: C 66.86, H 9.31, N 7.80; found: C 66.65, H 9.78, N 7.98.

DTPA-BC_{14}PheA: Yield: 0.81 g, 86%; ^{1}H NMR (400 MHz, CD_3OD, 25 °C, TMS): $\delta=0.91$ (t, 6H, CH_3), 1.28 (m, 52H, alkyl CH_2), 2.36, 2.50 (t, 8H, N-CH_2-CH_2-N), 2.91, 3.02, 3.56 (s, 10H, N-CH_2-C(O)), 7.11 (d, 4H, phenyl C*H*), 7.48 ppm (d, 4H, phenyl C*H*); IR: $\tilde{\nu}_{max}=1626$ (C=O free acid), 1529 cm^{-1} (C=O amide); ESI-MS: m/z calcd for $C_{54}H_{89}N_5O_8$: 937.3 $[M+H]^{+}$, 959.3 $[M+Na]^{+}$, found 938.0 $[M+H]^{+}$, 959.4 $[M+Na]^{+}$; elemental analysis calcd (%) for $C_{54}H_{89}N_5O_8$: C 69.27, H 9.58, N 7.48; found: C 69.55, H 9.65, N 7.53.

Dy-DTPA-BC_{12}PheA (Dy5) and Dy-DTPA-BC_{14}PheA (Dy6) complexes: The ligand (1 mmol, 1 equiv) was dissolved in pyridine (30 mL) and a solution of hydrated $DyCl_3$ salt (1.1 mmol, 1.1 equiv) in H_2O (1 mL) was added. The mixture was brought to 70 °C for 3 h after which the solvents were evaporated. The crude product was then heated at reflux in ethanol for one hour. The suspension was cooled to room temperature, the complex was filtered off and dried in vacuo at 50 °C. The absence of free lanthanide ions was checked with an arsenazo indicator.[19]

Dy^{III}-DTPA-BC_{12}PheA (Dy5): Yield: 52%. IR: $\tilde{\nu}_{max}=1596$ (COO^{-} asym. stretch), 1514 (amide II), 1391 cm^{-1} (COO^{-} sym. stretch); UV/Vis (water): λ_{max} (ε): 263 nm ($39\,000\ cm^{-1}M^{-1}$); ESI-MS: m/z calcd for $C_{50}H_{78}DyN_5O_8$: 1062.7 $[M+Na]^{+}$; found: 1062.8 $[M+Na]^{+}$; elemental analysis calcd (%) for $C_{50}H_{78}DyN_5O_8{\cdot}H_2O$: C 56.58, H 7.62, N 6.62; found: C 56.17, H 7.75, N 6.59.

Dy^{III}-DTPA-BC_{14}PheA (Dy6): Yield: 61%. IR: $\tilde{\nu}_{max}=1595$ (COO^{-} asym. stretch), 1514 (amide II), 1392 cm^{-1} (COO^{-} sym. stretch); UV/Vis (water): λ_{max} (ε): 263 nm ($40\,950\ cm^{-1}M^{-1}$); ESI-MS: m/z calcd for $C_{54}H_{86}DyN_5O_8$: 1118.8 $[M+Na]^{+}$, found 1120.4 $[M+Na]^{+}$; elemental analysis calcd (%) for $C_{54}H_{86}DyN_5O_8{\cdot}H_2O$: C 58.23, H 7.96, N 6.29; found: C 58.02, H 8.11, N 6.34.

Preparation of micelles:[17c] 1,2-Dipalmitoyl-*sn*-glycero-3-phosphocholine (DPPC, 225 mg, 0.3 mmol, 12 equiv) and the amphiphilic complex (25 mg, ±0.025 mmol, 1 equiv) were dissolved in a 1:1 chloroform/methanol solution (50 mL). After evaporation of the solvents, a thin film was obtained which was rehydrated with hot water (5 mL, 70 °C). To improve

the solubility, the suspension was sonicated in a 180 W sonicator with a thermostatic bath at 65 °C for 15 min. Polyoxyethylene sorbitan monooleate or Tween 80 (75 mg, 0.06 mmol, 2.4 equiv) was added as a surfactant followed by another 15 min of sonication to fulfill the process of micelle formation. Water was evaporated while slowly reducing the pressure.

Acknowledgements

E.D. and T.N.P.V. acknowledge the IWT Flanders (Belgium) and the FWO Flanders (project G.0412.09) for financial support. CHN microanalysis was performed by Mr. Dirk Henot. ESI-MS measurements were performed with the help of Mr. Dirk Henot and Mr. Bert Demarsin and ICP-OES measurements were performed by Ms. Elvira Vassilieva (Department of Earth and Environmental Sciences). Mr. Karel Duerinckx is acknowledged for his help with the NMR measurements. L.V.E., S.L., and R.N.M. thank the ARC Programs of the French Community of Belgium, the FNRS (Fonds National de la Recherche Scientifique), the support and sponsorship concerted by COST Actions (D38 and TD1004) and the EMIL program.

[1] P. Caravan, J. J. Ellison, T. J. McMurry, R. B. Lauffer, *Chem. Rev.* **1999**, *99*, 2293–2352.

[2] a) A. J. L. Villaraza, A. Bumb, M. W. Brechbiel, *Chem. Rev.* **2010**, *110*, 2921–2959; b) P. Lebdušková, J. Kotek, P. Hermann, L. Vander Elst, R. N. Muller, I. Lukeš, J. A. Peters, *Bioconjugate Chem.* **2004**, *15*, 881–889; c) C.-H. Huang, K. Nwe, A. Al Zaki, M. W. Brechbiel, A. Tsourkas, *ACS Nano* **2012**, *6*, 9416–9424; d) Y. Li, M. Beija, S. Laurent, L. Vander Elst, R. N. Muller, H. T. T. Duong, A. B. Lowe, T. P. Davis, C. Boyer, *Macromolecules* **2012**, *45*, 4196–4204; e) K. Luo, G. Liu, W. She, Q. Wang, G. Wang, B. He, H. Ai, Q. Gong, B. Song, Z. Gu, *Biomaterials* **2011**, *32*, 7951–7960.

[3] a) M. Zhen, J. Zheng, L. Ye, S. Li, C. Jin, K. Li, D. Qiu, H. Han, C. Shu, Y. Yang, C. Wang, *ACS Appl. Mater. Interfaces* **2012**, *4*, 3724–3729; b) T. N. Parac-Vogt, K. Kimpe, S. Laurent, L. Vander Elst, C. Burtea, F. Chen, R. N. Muller, Y. C. Ni, A. Verbruggen, K. Binnemans, *Chem. Eur. J.* **2005**, *11*, 3077–3086; c) P. Caravan, *Acc. Chem. Res.* **2009**, *42*, 851–862; d) C. Henoumont, V. Henrotte, S. Laurent, L. Vander Elst, R. N. Muller, *J. Inorg. Biochem.* **2008**, *102*, 721–730.

[4] a) F. Kielar, L. Tei, E. Terreno, M. Botta, *J. Am. Chem. Soc.* **2010**, *132*, 7836–7837; b) T. N. Parac-Vogt, K. Kimpe, S. Laurent, C. Piérart, L. Vander Elst, R. N. Muller, K. Binnemans, *Eur. J. Inorg. Chem.* **2004**, 3538–3543; c) C. Vanasschen, N. Bouslimani, D. Thonon, J. F. Desreux, *Inorg. Chem.* **2011**, *50*, 8946–8958.

[5] F. Hu, *Nanoscale* **2012**, *4*, 6235.

[6] a) S. L. Jeon, M. K. Chae, E. J. Jang, C. Lee, *Chem. Eur. J.* **2013**, *19*, 4217–4222; b) F. Ye, *Contrast Media Mol. Imaging* **2012**, *7*, 460–468; c) S. Soenen, *Contrast Media Mol. Imaging* **2009**, *4*, 207–219; d) H. B. Na, I. C. Song, T. Hyeon, *Adv. Mater.* **2009**, *21*, 2133–2148.

[7] a) A. Louie, *Chem. Rev.* **2010**, *110*, 3146–3195; b) L. Frullano, T. J. Meade, *J. Biol. Inorg. Chem.* **2007**, *12*, 939–949; c) D. Jańczewski, Y. Zhang, G. K. Das, D. K. Yi, P. Padmanabhan, K. K. Bhakoo, T. T. Y. Tan, S. T. Selvan, *Microsc. Res. Tech.* **2011**, *74*, 563–576.

[8] a) C. Bernhard, C. Goze, Y. Rousselin, F. Denat, *Chem. Commun.* **2010**, *46*, 8267–8269; b) A. Keliris, T. Ziegler, R. Mishra, R. Pohmann, M. G. Sauer, K. Ugurbil, J. Engelmann, *Bioorg. Med. Chem.* **2011**, *19*, 2529–2540.

[9] a) T. Koullourou, L. Natrajan, H. Bhavsar, S. J. A. Pope, J. Feng, R. Kauppinen, J. Narvainen, R. Shaw, E. Scales, A. Kenwright, S. Faulkner, *J. Am. Chem. Soc.* **2008**, *130*, 2178–2179; b) G. Dehaen, S. V. Eliseeva, K. Kimpe, S. Laurent, L. Vander Elst, R. N. Muller, W. Dehaen, K. Binnemans, T. N. Parac-Vogt, *Chem. Eur. J.* **2012**, *18*, 293–302; c) G. Dehaen, S. V. Eliseeva, P. Verwilst, S. Laurent, L. Vander Elst, R. N. Muller, W. De Borggraeve, K. Binnemans, T. N. Parac-Vogt, *Inorg. Chem.* **2012**, *51*, 8775–8783; d) E. Debroye, G. Dehaen, S. V. Eliseeva, S. Laurent, L. Vander Elst, R. N. Muller, K. Binnemans, T. N. Parac-Vogt, *Dalton Trans.* **2012**, *41*, 10549–10556.

[10] a) N. Kamaly, T. Kalber, G. Kenny, J. Bell, M. Jorgensen, A. Miller, *Org. Biomol. Chem.* **2010**, *8*, 201–211; b) S. J. Soenen, G. V. Velde, A. Ketkar-Atre, U. Himmelreich, M. De Cuyper, *Wiley Interdiscip. Rev. Nanomed. Nanobiotechnol.* **2011**, *3*, 197–211.

[11] W. J. Rieter, J. S. Kim, K. M. L. Taylor, H. An, W. Lin, T. Tarrant, W. Lin, *Angew. Chem.* **2007**, *119*, 3754–3756; *Angew. Chem. Int. Ed.* **2007**, *46*, 3680–3682.

[12] a) P. Howes, M. Green, A. Bowers, D. Parker, G. Varma, M. Kallumadil, M. Hughes, A. Warley, A. Brain, R. Botnar, *J. Am. Chem. Soc.* **2010**, *132*, 9833–9842; b) S. Ronchi, M. Colombo, P. Verderio, S. Mazzucchelli, F. Corsi, C. De Palma, R. Allevi, E. Clementi, D. Prosperi, *AIP Conf. Proc.* **2010**, *1275*, 102–105; c) D. Bhattacharya, M. Das, D. Mishra, I. Banerjee, S. K. Sahu, T. K. Maiti, P. Pramanik, *Nanoscale* **2011**, *3*, 1653–1662; d) Y. Chen, H. Chen, S. Zhang, F. Chen, L. Zhang, J. Zhang, M. Zhu, H. Wu, L. Guo, J. Feng, J. Shi, *Adv. Funct. Mater.* **2011**, *21*, 270–278.

[13] a) F. A. Rojas-Quijano, E. T. Benyó, G. Tircsó, F. K. Kálmán, Z. Baranyai, S. Aime, A. D. Sherry, Z. Kovács, *Chem. Eur. J.* **2009**, *15*, 13188–13200; b) G. Tallec, P. H. Fries, D. Imbert, M. Mazzanti, *Inorg. Chem.* **2011**, *50*, 7943–7945; c) C. S. Bonnet, F. Buron, F. Caillé, C. M. Shade, B. Drahoš, L. Pellegatti, J. Zhang, S. Villette, L. Helm, C. Pichon, F. Suzenet, S. Petoud, É. Tóth, *Chem. Eur. J.* **2012**, *18*, 1419–1431; d) S. L. C. Pinho, H. Faneca, C. F. G. C. Geraldes, J. Rocha, L. D. Carlos, M.-H. Delville, *Eur. J. Inorg. Chem.* **2012**, 2828–2837; e) E. Debroye, S. Eliseeva, S. Laurent, L. Vander Elst, S. Petoud, R. N. Muller, T. N. Parac-Vogt, *Eur. J. Inorg. Chem.* **2013**, 2629–2639.

[14] C. M. Andolina, P. J. Klemm, W. C. Floyd, J. M. J. Fréchet, K. N. Raymond, *Macromolecules* **2012**, *45*, 8982–8990.

[15] a) L. Vander Elst, A. Roch, P. Gillis, S. Laurent, F. Botteman, J. W. M. Bulte, R. N. Muller, *Magn. Reson. Med.* **2002**, *47*, 1121–1130; b) G. K. Das, N. J. J. Johnson, J. Cramen, B. Blasiak, P. Latta, B. Tomanek, F. C. J. M. van Veggel, *J. Phys. Chem. Lett.* **2012**, *3*, 524–529; c) M. Norek, E. Kampert, U. Zeitler, J. A. Peters, *J. Am. Chem. Soc.* **2008**, *130*, 5335–5340; d) P. Caravan, M. T. Greenfield, J. W. M. Bulte, *Magn. Reson. Med.* **2001**, *46*, 917–922.

[16] a) A. Zhang, J. Zhang, Q. Pan, S. Wang, H. Jia, B. Xu, *J. Lumin.* **2012**, *132*, 965–971; b) Y. Bi, X.-T. Wang, W. Liao, X. Wang, R. Deng, H. Zhang, S. Gao, *Inorg. Chem.* **2009**, *48*, 11743–11747.

[17] a) A. Accardo, D. Tesauro, L. Aloj, C. Pedone, G. Morelli, *Coord. Chem. Rev.* **2009**, *253*, 2193–2213; b) W. J. M. Mulder, G. J. Strijkers, G. A. F. van Tilborg, A. W. Griffioen, K. Nicolay, *NMR Biomed.* **2006**, *19*, 142–164; c) K. Kimpe, T. N. Parac-Vogt, S. Laurent, C. Piérart, L. Vander Elst, R. N. Muller, K. Binnemans, *Eur. J. Inorg. Chem.* **2003**, 3021–3027; d) S. Aime, *Inorg. Chem.* **1994**, *33*, 4707.

[18] S. Laurent, T. N. Parac-Vogt, K. Kimpe, C. Thirifays, K. Binnemans, R. N. Muller, L. Vander Elst, *Eur. J. Inorg. Chem.* **2007**, 2061–2067.

[19] H. Onishi, K. Sekine, *Talanta* **1972**, *19*, 473–478.

[20] a) S. Aime, F. Benetollo, G. Bombieri, S. Colla, M. Fasano, S. Paoletti, *Inorg. Chim. Acta* **1997**, *254*, 63–70; b) Y.-M. Wang, Y.-J. Wang, R.-S. Sheu, G.-C. Liu, W.-C. Lin, J.-H. Liao, *Polyhedron* **1999**, *18*, 1147–1152.

[21] a) N. Fretellier, *Invest. Radiol.* **2011**, *46*, 292; b) T. Frenzel, *Invest. Radiol.* **2008**, *43*, 817; c) S. K. Morcos, *Br. J. Radiol.* **2007**, *80*, 73–76.

[22] W. Jivaramonaikul, P. Rashatasakhon, S. Wanichwecharungruang, *Photochem. Photobiol. Sci.* **2010**, *9*, 1120–1125.

[23] a) G. Bergamini, P. Ceroni, M. Maestri, S.-K. Lee, J. van Heyst, F. Vögtle, *Inorg. Chim. Acta* **2007**, *360*, 1043–1051; b) I. B. Berlman, *Handbook of Fluorescence Spectra of Aromatic Molecules*, Academic Press, New York, **1971**.

[24] R. Nandy, S. Sankararaman, *Beilstein J. Org. Chem.* **2010**, *6*, 992–1001.

[25] K. Driesen, R. Van Deun, C. Görller-Walrand, K. Binnemans, *Chem. Mater.* **2004**, *16*, 1531–1535.

[26] F. J. Steemers, W. Verboom, D. N. Reinhoudt, E. B. van der Tol, J. W. Verhoeven, *J. Am. Chem. Soc.* **1995**, *117*, 9408–9414.

[27] W. T. Carnall, P. R. Fields, K. Rajnak, *J. Chem. Phys.* **1968**, *49*, 4412–4423.
[28] a) T. Kimura, Y. Kato, *J. Alloys Compd.* **1998**, *275*, 806–810; b) W. D. Horrocks, Jr., D. R. Sudnick, *J. Am. Chem. Soc.* **1979**, *101*, 334–340.
[29] a) J. Feng, H.-J. Zhang, S.-Y. Song, Z.-F. Li, L.-N. Sun, Y. Xing, X.-M. Guo, *J. Lumin.* **2008**, *128*, 1957–1964; b) Z.-F. Li, L. Zhou, J.-B. Yu, H.-J. Zhang, R.-P. Deng, Z.-P. Peng, Z.-Y. Guo, *J. Phys. Chem. C* **2007**, *111*, 2295–2300; c) S. Quici, M. Cavazzini, G. Marzanni, G. Accorsi, N. Armaroli, B. Ventura, F. Barigelletti, *Inorg. Chem.* **2005**, *44*, 529–537; d) S. Petoud, S. M. Cohen, J.-C. G. Bünzli, K. N. Raymond, *J. Am. Chem. Soc.* **2003**, *125*, 13324–13325.
[30] E. Debroye, S. V. Eliseeva, S. Laurent, L. Vander Elst, R. N. Muller, T. N. Parac-Vogt, *Inorg. Chem.* **2013**, 2629–2639.
[31] a) I. Hemmilä, S. Dakubu, V.-M. Mukkala, H. Siitari, T. Lövgren, *Anal. Biochem.* **1984**, *137*, 335–343; b) I. Hemmilá, V.-M. Mukkala, *Crit. Rev. Clin. Lab. Sci.* **2001**, *38*, 441–519; c) J. A. Keelan, J. T. France, P. M. Barling, *Clin. Chem.* **1987**, *33*, 2292–2295; d) I. Hemmilä, V. Laitala, *J. Fluoresc.* **2005**, *15*, 529–542.
[32] a) S. Viswanathan, Z. Kovacs, K. N. Green, S. J. Ratnakar, A. D. Sherry, *Chem. Rev.* **2010**, *110*, 2960–3018; b) J. A. Peters, J. Huskens, D. J. Raber, *Prog. Nucl. Magn. Reson. Spectrosc.* **1996**, *28*, 283–350.
[33] D. F. Eaton, *Pure Appl. Chem.* **1988**, *60*, 1107–1114.
[34] F. Jasanada, F. Nepveu, *Tetrahedron Lett.* **1992**, *33*, 5745–5748.

Received: June 24, 2013
Published online: October 10, 2013

